



Synthesis and in vitro antimycobacterial and antileishmanial activities of hydroquinone-triazole hybrids

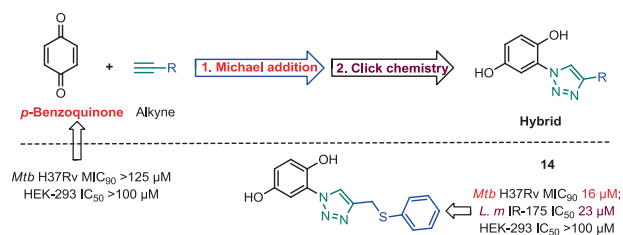
Chris-Marie Horn¹ · Janine Aucamp² · Frans J. Smit² · Ronnett Seldon³ · Audrey Jordaan⁴ · Digby F. Warner^{4,5} · David D. N'Da^{1b}

Received: 27 February 2020 / Accepted: 27 April 2020
© Springer Science+Business Media, LLC, part of Springer Nature 2020

Abstract

Infectious diseases such as tuberculosis and leishmaniasis are leading causes of human death. One of the major factors contributing to the poor control of these diseases is primarily the reduced effectiveness of the existing chemotherapies as result of the increasing rise of multidrug-resistant strains of their causative agents. This leads to the imperative need to develop new and effective drugs. In search for such agents, a series of hydroquinone-triazole hybrids was investigated. The design, synthesis, and biological activities against the human virulent H37Rv strain of *Mycobacterium tuberculosis* (*Mtb*) and *Leishmaniasis major* (*L. major*), causative pathogen of human cutaneous leishmaniasis, are herein reported. The hybrids were synthesized following a two-step process Michael addition and Click chemistry. They were found to be noncytotoxic toward human kidney embryonic cells but expressed poor cellular antileishmanial and antimycobacterial activities. Hybrid **14**, 2-[4-[(phenylsulfanyl)methyl]-1H-1,2,3-triazol-1-yl]benzene-1,4-diol, was the most active among synthesized molecules, with MIC₉₀ 16 and IC₅₀ 23 μM against *Mtb* and *L. major* parasite, respectively, but had a poor safety profile, being as toxic to mammalian cells as to mycobacteria and parasites. Thus, compound **14** did not stand as potential anti-infective hit for further investigation. Future endeavor will focus on the investigation of more rigid and flexible hybrids of both scaffolds in order to assess the impact a spacer might have on their biological activity.

Graphical Abstract



Supplementary information The online version of this article (<https://doi.org/10.1007/s00044-020-02553-0>) contains supplementary material, which is available to authorized users.

✉ David D. N'Da
david.nda@nwu.ac.za

- 1 Pharmaceutical Chemistry, School of Pharmacy, North-West University, Potchefstroom 2520, South Africa
- 2 Centre of Excellence for Pharmaceutical Sciences (Pharmacem), North-West University, Potchefstroom 2520, South Africa
- 3 SAMRC Drug Discovery and Development Research Unit,

University of Cape Town, Cape Town 7700, South Africa

- 4 SAMRC/NHLS/UCT Molecular Mycobacteriology Research Unit, Department of Pathology and Institute of Infectious Disease and Molecular Medicine, Faculty of Health Sciences, University of Cape Town, Cape Town 7925, South Africa
- 5 Wellcome Centre for Clinical Infectious Diseases Research in Africa, University of Cape Town, Cape Town 7925, South Africa

Keywords Infectious diseases · Drug research · Molecular hybridization · Quinone · Triazole · Cyclizations

Introduction

After decades of effective chemotherapeutic treatment, tuberculosis (TB) still affects and kills millions of people each year. TB is one of the top ten causes of mortality worldwide (WHO 2018a) and is the leading cause of death from a single infectious disease, surpassing human immunodeficiency virus (WHO 2018b). In 2017 alone, ten million people contracted TB and 1.6 million fatalities were registered, of which more than 95% occurred in low- and middle-income countries (CDC 2018a; WHO 2018a). Majority of the estimated incidence cases occurred in South-East Asia (44%), and Africa (25%) (WHO 2018c), making TB a disease of the developing world.

The use of antitubercular drugs is currently the only viable option available for the control of TB, as other control measures (such as the use of Bacillus Calmette–Guérin vaccine and TB chemoprophylaxis) appear to be unsatisfactory (du Toit et al. 2006). The existing antitubercular drugs, although of immense value in controlling the disease, have several limitations with the most important shortcoming being the emergence of drug-resistant TB strains that renders the frontline drugs in particular, less active (Amir et al. 2014).

Furthermore, these drugs possess excessive adverse side effects, which are alleviated through additional therapies, incurring more expenses for patients. Overall, the current TB treatment regimens, apart from being less effective and safe, are becoming unaffordable for patients in the developing countries who need them most. This emphasizes the search for new, effective, and cheap anti-TB alternatives.

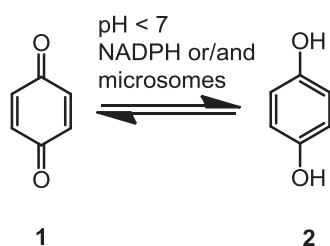
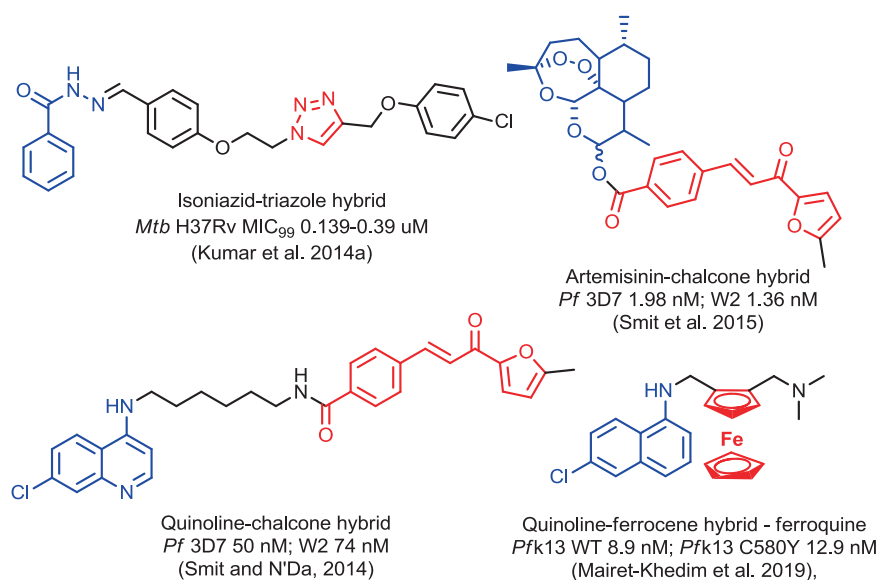
Leishmaniasis, on the other hand, is one of the seven most important tropical diseases and presents a serious world health challenge. In 2017 alone, the death toll due to the most common form of the disease (cutaneous leishmaniasis (CL)) was 20,000–30,000 while 700,000–1 million new cases were reported (WHO 2018e). This infectious disease is widely distributed across 97 countries mainly in Africa, Asia and Latin America (WHO 2018d). Leishmaniasis is a vector-borne disease that is transmitted by *phlebotomine* sand flies and caused by the obligate intracellular protozoa of the genus *Leishmania* (WHO 2019f). There are three clinical forms of leishmaniasis, namely mucocutaneous (MCL), CL (Aleppo boil), and visceral leishmaniasis (VL, kala azar, black fever) (WHO 2019f). The latter affects bone marrow, liver, and spleen (to a larger extent), presenting symptoms such as fever, hepatosplenomegaly, pancytopenia, and weight loss, which result in death if left untreated. Most leishmaniasis related fatalities are caused

by VL (CDC 2019; WHO 2019g). CL, on the other hand, is the most common form, results in mutilation and esthetic/social stigma (as a result of multiple lesions) (WHO 2019g) while MCL causes partial or complete destruction of soft and hard tissues of the palate, pharynx, and nose (WHO 2019g).

Treatment of leishmaniasis is limited to the use of a handful of drugs including antimonials, paromomycin, miltefosine, pentamidine, and amphotericin B (Aronson et al. 2017; Torres-Guerrero et al. 2017). These therapies are administered by either intravenous or intramuscular (painful) routes, and often not consecutively during the treatment period due to severe adverse effects. Resistance to antimonial drugs has been established (Hadighi et al. 2006; Ponte-Sucre et al. 2017) while emergence of resistance against miltefosine (Deep et al. 2017; Ponte-Sucre et al. 2017) and amphotericin B (Brotherton et al. 2014; Ponte-Sucre et al. 2017) is proven in experimental settings on laboratory strains and field isolates, which may be indicative of the looming loss of these two drugs. Monotherapy of pentamidine is near discontinuation due to the loss of efficacy and high toxicity while therapy of paromomycin is associated with hepatotoxicity (Ansari et al. 2017). Thus, the development of new antileishmanial agents with reduced adverse effects and less invasive administration routes is highly desired to treat this infection.

A promising strategy for the discovery of such drugs is molecular hybridization, which is defined as the covalent chemical linking of two or more pharmacophores to create a single new chemical entity, with two structural domains and biological functions that may act on different targets (dual drug action) or wherein one part may equipose the side effects caused by another part (Kumar et al. 2014a; Smit et al. 2015). Hybrid molecules may have improved efficacy and affinity (Viegas-Junior et al. 2007), and are therapeutically and medicinally more effective than individual components (Smit and N'Da 2014). Structures of few promising hybrid compounds (Kumar et al. 2014a; Smit and N'Da 2014; Smit et al. 2015) and hybrid drug candidate, ferroquine (Mairet-Khedim et al. 2019), are shown in Fig. 1.

1,2,3-Triazole is a five-member *N*-heterocyclic scaffold (Ali et al. 2017). Synthetic compounds containing this moiety have been found with an array of biological properties inter alia antitubercular (Boechat et al. 2011) due to it having favorable physicochemical features such as hydrogen bonding capability, moderate dipole, rigidity etc. (Zhang et al. 2017). Some of these compounds, similarly to isoniazid, exert their antitubercular action by inhibiting microbial cell wall synthesis through blocking of lipid biosynthesis (Kumar et al. 2014a; Zhang et al. 2017).

Fig. 1 Structures of hybrid compounds**Scheme 1** Interconversion of benzoquinone (1) to hydroquinone (2) with conditions favouring the reduction of 1

Several 1,2,3-triazole containing drugs are currently on the market (Smit et al. 2019).

1,4-Benzoquinone (BQ) is the envisaged partner pharmacophore to 1,2,3-triazole investigated in this study. The reduction of BQ to hydroquinone (HQ) via semiquinone, occurs spontaneously and by the action of various enzymes in a biological system (Scheme 1), the same also being valid for the reverse reaction (HQ \leftrightarrow BQ) (McGregor 2007; Netherlands HCot 2012). In an aqueous solution, 1,4-BQ is reduced to HQ at a significant rate, further stimulated by the presence of nicotinamide adenine dinucleotide phosphate hydrogen (NADPH), and more so in the presence of NADPH and microsomes (a complete microsomal system). In contrast, the autoxidation of HQ is slow, even further slower in the presence of NADPH, and stopped entirely by a complete microsomal system. Therefore, in an aqueous medium, the main direction of conversion is the reduction of BQ, with the complete reduction to HQ taking place within 5 min in a complete system (NADPH and microsomes) (Souček et al. 2000). HQ autoxidation in an aqueous medium is pH-dependent, occurring rapidly under alkaline conditions and slowly under acidic conditions (McGregor 2007; Netherlands HCot 2012).

BQ and HQ are metabolites of each other, with the interconversion rate dependent on prevailing local

conditions. Due to this constant interconversion in an aqueous medium, we justified synthesizing HQ-linked 1,2,3-triazoles. Pharmacological properties of BQ compounds include anti-inflammatory (Sagnou et al. 2009), anticancer (Lindsey et al. 2004; Tasdemir et al. 2006), antiviral and antimalarial (Tasdemir et al. 2006), antimycobacterial (Jyoti et al. 2016; Tasdemir et al. 2006), and antileishmanial (Valderrama et al. 2005). Thus, the available literature suggests that BQ and HQ moieties possess both antimycobacterial and antileishmanial activities.

Quinones have a number of biological activities and, although the precise mechanism of action is not fully understood, most of their effects are attributed to redox cycling and the generation of reactive oxygen species (ROS) such as superoxide and hydrogen peroxide that damage cells (Tran et al. 2004). ROS directly combat infection by signaling cascades to prompt other protective cellular measures (such as apoptosis) or by causing severe oxidative stress within cells (Tasdemir et al. 2006). Likewise, HQ might affect *Mtb* and *Leishmania* by disrupting intracellular components such as RNA, DNA, internal proteins, and other organelles.

We herein report the synthesis and in vitro antimycobacterial and antileishmanial activities of a small library of hybrids formed from HQ and 1,2,3-triazole scaffolds.

Materials and methods

Materials

Para-Benzoquinone (*p*-BQ), sodium azide (NaN₃), β -cyclodextrin, sodium ascorbate (NaAsc), copper ascorbate (CuAsc), copper sulfate (CuSO₄), 1-ethynylcyclohexanol,

1-hexyne, 1-heptyne, 1-octyne, 1-decyne, phenylacetylene, tetrahydro-2-(2-propynyloxy)-2H-pyran, methyl propiolate, propargyl alcohol, 4-ethynyltoluene, phenyl propargyl sulfide, sodium nitrite (NaNO_2) magnesium sulfate (MgSO_4), sodium bicarbonate (NaHCO_3) were purchased from Sigma-Aldrich (South Africa). All solvents used, methanol (MeOH), acetone, tetrahydrofuran (THF), ethyl acetate (EtOAc), dichloromethane (DCM), hexane, dimethyl sulfide (DMSO) were purchased from Associated Chemical Enterprises (South Africa) or from Sigma-Aldrich (South Africa). All chemicals and reagents were of analytical grade and were used without further purification. For inert reactions, DCM was distilled over calcium hydride and stored over 3 Å molecular sieves.

General procedures

The ^1H and ^{13}C nuclear magnetic resonance (NMR) spectra were recorded on a Bruker AvanceTM III 600 spectrometer at a frequency of 150 MHz, respectively, in deuterated DMSO ($\text{DMSO-}d_6$). Chemical shifts are reported in parts per million (ppm) with the residual protons of the solvent as reference (^1H NMR (600 MHz, $\text{DMSO-}d_6$) δ 2.5 and ^{13}C NMR (151 MHz, $\text{DMSO-}d_6$) δ ^{13}C 40). The splitting pattern abbreviations are as follows: s (singlet), d (doublet), dd (doublet of doublet), t (triplet), q (quartet), p (pentet), and m (multiplet).

High resolution mass spectrometry (HRMS) was recorded on a Bruker MicroTOF Q II mass spectrometer that had an atmospheric pressure chemical ionization (APCI) source set at 200 °C using Bruker Compass DataAnalysis 4.0 software. A full scan, ranging between 50–1500 m/z , was generated at a capillary voltage of 4500 V, an end plate offset voltage of 500 V, and a collision cell radio frequency voltage of 100 Vpp.

Fourier Transformed Infrared (FTIR) spectra were recorded on a Bruker Alpha-P FTIR instrument. Melting points (m.p.) were determined with a BÜCHI m.p. B-545 instrument and were uncorrected. Thin layer chromatography (TLC) was performed using silica gel plates (60F₂₅₄), acquired from Merck (South Africa).

High performance liquid chromatography (HPLC) analysis of the final compounds was performed to determine purity. An Agilent 1100 HPLC system equipped with a quaternary pump and an Agilent 1100 series diode array detector were utilized. HPLC-grade acetonitrile (Merck) and Milli-Q water (Millipore) were used for chromatography. A Venusil XBP C-18 column (4.60 × 150 mm, 5 μm), with an initial mobile phase (70% Milli-Q water: 30% acetonitrile), was employed at a flow rate of 1 mL/min. The concentration of acetonitrile in the mobile phase was linearly increased over a period of 5 min to a final concentration of 85%. The time allowed for equilibration

between runs was 5 min and the duration of each HPLC run was 15 min. The concentration of the test compounds injected varied (20 μL of 1 mM to 20 μL of 0.25 mM). The eluent was monitored at wavelengths of 210, 254, and 300 nm.

Synthesis

2-Azidobenzene-1,4-diol **3**

The intermediate was prepared by adopting the literature reported (Couladouros et al. 1997) method with minor modifications as illustrated in Scheme 2, step i.

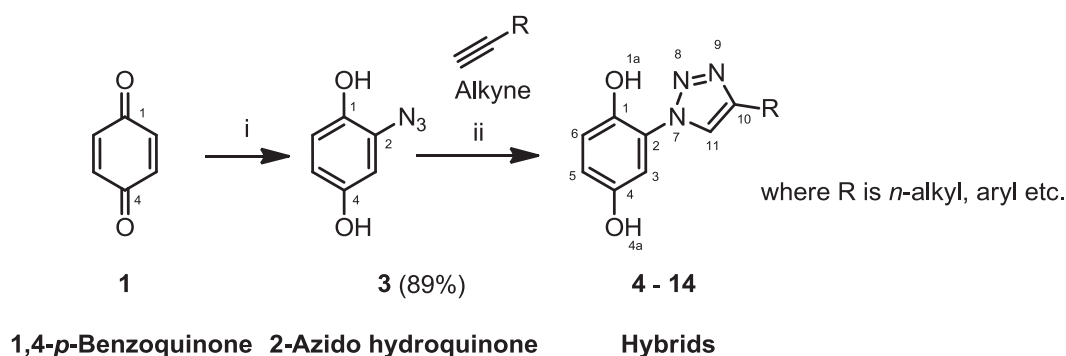
In a single neck round bottom flask, *p*-BQ **1** (18.6 mmol, 2.0 g, 1 eq.) was dissolved in MeOH (80 mL) upon stirring at -78 °C (on dry ice), and flushed with argon. NaN_3 , (74.0 mmol, 4.8 g, 4.00 eq.) was dissolved in MeOH (30 mL) and pH of the solution was adjusted to 4 using 1 M HCl then added portion wise to BQ solution at regular intervals (5 × 10 min). The resulting mixture was continued stirring at -78 °C under argon for another 1.5 h to produce the azide intermediate **3**. The progress of the reaction was monitored using TLC. Upon completion, the solvent was evaporated and NaHCO_3 (50 mL) was added to the residue. The crude organic layer was successively extracted with EtOAc (150 mL) and DCM (150 mL). The resulting organic layers were dried over anhydrous MgSO_4 , filtered, evaporated to dryness. The resulting residue was purified by column chromatography on silica gel eluting DCM/MeOH (9:1, v/v) to yield **3**.

Dark brown powder; ^1H NMR (600 MHz, $\text{DMSO-}d_6$) δ 9.21 (s, 1H, H-1a), 8.96 (s, 1H, H-4a), 6.67 (d, $J = 2.8$ Hz, 1H, H-3), 6.41 (dd, $J = 8.7, 2.8$ Hz, 1H, H-5), 6.33 (d, $J = 8.7$ Hz, 1H, H-6). ^{13}C NMR (151 MHz, $\text{DMSO-}d_6$) δ 150.77 (C-4), 143.08 (C-1), 125.99 (C-2), 117.43 (C-5), 112.80 (C-6), 107.54 (C-3).

Synthesis of hybrids 4–14

Compounds **4–14** were prepared in accordance with the general procedure (Dixit et al. 2012) depicted in Scheme 2 step ii, and is described as follows:

In a single neck flat bottom flask, alkyne (1.20 eq.) was mixed in THF (6 mL), MeOH (6 mL), and distilled H_2O (6 mL). β -Cyclodextrin (0.02 eq.), NaAsc (0.20 eq.), **3** (1.00 eq.), and CuSO_4 (0.10 eq.) were consecutively added to the flask. The reaction was left to stir at room temperature for 28–29 h. The progress of the reaction was monitored using TLC. Afterwards, the solvent was evaporated, the product was extracted with hot EtOAc, washed with NaHCO_3 , dried over anhydrous MgSO_4 , and recrystallized using hot EtOAc and hexane, to produce the desired pure compound.



Compd.	R	Yield (%)	Compd.	R	Yield (%)
4		42	10		69
5		47	11		29
6		46	12		43
7		52	13		45
8		70	14		23
9		58			

Scheme 2 General reaction procedure of hydroquinone-1,2,3-triazole hybrids. Reagents and conditions: (i) **1**: *p*-benzoquinone (1.00 eq.), MeOH, -78°C , NaN_3 (4.00 eq.)/MeOH sol. (pH~4), 1.5 h. (ii) **4-14**:

alkyne (1.20 eq.), THF, MeOH, H_2O , β -cyclodextrin (0.02 eq.), sodium ascorbate (0.20 eq.), **3** (1 eq.), and CuSO_4 (0.10 eq.), r.t, 28 h

2-(4-Butyl-1*H*-1,2,3-triazol-1-yl)benzene-1,4-diol **4**

The reaction with 1-hexyne afforded hybrid **4** as brown crystals; m.p. $159.4\text{--}162.4^{\circ}\text{C}$; IR ν_{max} : 3185, 3079, 2955, 2579, 1614, 1533, 1467, 1432, 1407 cm^{-1} ; ^1H NMR (600 MHz, $\text{DMSO-}d_6$) δ 9.71 (s, 1H, H-4a), 9.25 (s, 1H, H-1a), 8.21 (s, 1H, H-11), 7.06 (d, $J = 2.8$ Hz, 1H, H-3), 6.92 (d, $J = 8.9$ Hz, 1H, H-6), 6.74 (dd, $J = 8.9, 2.8$ Hz, 1H, H-5), 2.69 (t, $J = 7.6$ Hz, 2H, H-12), 1.68–1.58 (m, 2H, H-13), 1.41–1.31 (m, 2H, H-14), 0.92 (t, $J = 15$ Hz, 3H, H-15); ^{13}C NMR (151 MHz, $\text{DMSO-}d_6$) δ 150.55 (C-1), 147.10 (C-4), 141.88 (C-10), 125.09 (C-2), 123.59 (C-11), 118.33 (C-5), 116.88 (C-3), 111.15 (C-6), 31.59 (C-13), 25.09 (C-12),

22.22 (C-14), 14.19 (C-15); HRMS (APCI) m/z : $[\text{M} + \text{H}]^+$ 234.1233 (Calc. for $\text{C}_{12}\text{H}_{16}\text{N}_3\text{O}_2$: 234.1198); purity (HPLC): 96%.

2-(4-Pentyl-1*H*-1,2,3-triazol-1-yl)benzene-1,4-diol **5**

The reaction with 1-heptyne gave hybrid **5** as off white crystals; m.p. $156.3\text{--}158.3^{\circ}\text{C}$; IR ν_{max} : 3180, 3080, 3024, 2588, 1614, 1529, 1473, 1439, 1380 cm^{-1} ; ^1H NMR (600 MHz, $\text{DMSO-}d_6$) δ 9.71 (s, 1H, H-4a), 9.24 (s, 1H, H-1a), 8.21 (s, 1H, H-11), 7.04 (d, $J = 2.9$ Hz, 1H, H-3), 6.92 (d, $J = 8.8$ Hz, 1H, H-6), 6.74 (dd, $J = 8.8, 2.9$ Hz, 1H, H-5), 2.68 (t, $J = 7.6$ Hz, 2H, H-12), 1.65 (p, $J = 7.6$ Hz, 2H,

H-13), 1.38–1.23 (m, 4H, H-14 & H-15), 0.88 ($J = 16$ Hz, 3H, H-16). ^{13}C NMR (151 MHz, DMSO- d_6) δ 150.56 (C-1), 147.16 (C-4), 141.88 (C-1), 125.10 (C-2), 123.57 (C-11), 118.35 (C-5), 116.89 (C-3), 111.15 (C-6), 31.34 (C-14), 29.12 (C-12), 25.38 (C-13), 22.34 (C-15), 14.38 (C-16); HRMS (APCI) m/z : $[\text{M} + \text{H}]^+$ 248.1411 (Calc. for $\text{C}_{13}\text{H}_{18}\text{N}_3\text{O}_2$: 248.1354); purity (HPLC): 97%.

2-(4-Hexyl-1H-1,2,3-triazol-1-yl)benzene-1,4-diol 6

The reaction with 1-octyne produced hybrid **6** as brown crystals; m.p. 157.4–159.5 °C; IR ν_{max} : 3180, 3081, 3020, 2583, 1614, 1472, 1388 cm^{-1} ; ^1H NMR (600 MHz, DMSO- d_6) δ 9.72 (s, 1H, H-4a), 9.24 (s, 1H, H-1a), 8.21 (s, 1H, H-11), 7.06 (dd, $J = 17.9, 2.9$ Hz, 1H, H-3), 6.93 (d, $J = 8.8$ Hz, 1H, H-6), 6.74 (dd, $J = 8.8, 2.9$ Hz, 1H, H-5), 2.69 (t, $J = 7.6$ Hz, 2H, H-12), 1.71–1.57 (m, 2H, H-13), 1.41–1.19 (m, 6H, H-14, -15, H-16), 0.87 (t, $J = 6.9$ Hz, 3H, H-17). ^{13}C NMR (151 MHz, DMSO- d_6) δ 150.55 (C-1), 147.14 (C-4), 141.87 (C-10), 125.08 (C-2), 123.59 (C-11), 118.33 (C-5), 116.88 (C-6), 111.13 (C-6), 31.50 (C-15), 29.42 (C-14), 28.79 (C-12), 25.42 (C-13), 22.53 (C-16), 14.43 (C-17); HRMS (APCI) m/z : $[\text{M} + \text{H}]^+$ 262.1561 (Calc. for $\text{C}_{14}\text{H}_{20}\text{N}_3\text{O}_2$: 262.1511); purity (HPLC): 96%.

2-(4-Octyl-1H-1,2,3-triazol-1-yl)benzene-1,4-diol 7

The reaction with 1-decyne gave hybrid **7** as off white crystals; m.p. 146.3–150.3 °C; IR ν_{max} : 3173, 3042, 2958, 2592, 1614, 1477, 1440, 1219 cm^{-1} ; ^1H NMR (600 MHz, DMSO- d_6) δ 9.71 (s, 1H, H-4a), 9.24 (s, 1H, H-1a), 8.21 (s, 1H, H-11), 7.04 (d, $J = 2.9$ Hz, 1H, H-3), 6.92 (d, $J = 8.8$ Hz, 1H, H-6), 6.73 (dd, $J = 8.8, 2.9$ Hz, 1H, H-5), 2.68 (t, $J = 7.6$ Hz, 2H, H-12), 1.67–1.56 (m, 2H, H-13), 1.38–1.14 (m, 10H, H-14... & H-18), 0.86 (t, $J = 7.6$ Hz, 3H, H-19). ^{13}C NMR (151 MHz, DMSO- d_6) δ 150.55 (C-1), 147.19 (C-4), 141.86 (C-10), 125.08 (C-2), 123.60 (C-11), 118.32 (C-5), 116.87 (C-3), 111.12 (C-6), 31.76 (C-17), 29.46 (C-16), 29.26–29.23 (C-15), 29.20 (C-14), 29.14 (C-12), 25.52–25.33 (C-13), 22.58 (C-18), 14.44 (C-19); HRMS (APCI) m/z : $[\text{M} + \text{H}]^+$ 290.1862 (Calc. for $\text{C}_{16}\text{H}_{24}\text{N}_3\text{O}_2$: 290.1824); purity (HPLC): 97%.

2-(4-Phenyl-1H-1,2,3-triazol-1-yl)benzene-1,4-diol 8

The reaction with phenylacetylene afforded hybrid **8** as brown–yellow crystals; m.p. 257.0–261.7 °C; IR ν_{max} : 3194, 3080, 3028, 2584, 1610 cm^{-1} ; ^1H NMR (600 MHz, DMSO- d_6) δ 9.81 (s, 1H, H-4a), 9.30 (s, 1H, H-1a), 8.91 (s, 1H, H-11), 7.89 (d, $J = 7.7$ Hz, 2H, H-13), 7.48 (t, $J = 7.7$ Hz, 2H, H-14), 7.37 (t, $J = 7.4$ Hz, 2H, H-15), 7.08 (d, $J = 2.9$ Hz, 1H, H-3), 6.98 (d, $J = 8.8$ Hz, 1H, H-6), 6.81 (dd, $J = 8.8, 2.9$ Hz, 1H, H-5). ^{13}C NMR (151 MHz, DMSO- d_6) δ

150.58 (C-1), 146.53 (C-4), 142.42 (C-10), 131.05 (C-12), 129.41 (C-2), 128.44 (C-14), 125.80 (C-15), 124.90 (C-13), 123.27 (C-11), 118.36 (C-5), 117.51 (C-6), 111.66 (C-6); HRMS (APCI) m/z : $[\text{M} + \text{H}]^+$ 254.0917 (Calc. for $\text{C}_{14}\text{H}_{12}\text{N}_3\text{O}_2$: 254.0885); purity (HPLC): 98%.

2-[4-(*p*-Tolyl)-1H-1,2,3-triazol-1-yl]benzene-1,4-diol 9

The reaction with 4-ethynyltoluene gave hybrid **9** as brown crystals; m.p. 275.7–276.7 °C; IR ν_{max} : 3188, 3074, 3025, 2581, 1615, 1474 cm^{-1} ; ^1H NMR (600 MHz, DMSO- d_6) δ 9.81 (s, 1H, H-4a), 9.31 (s, 1H, H-1a), 8.85 (s, 1H, H-11), 7.84 (d, $J = 8.1$ Hz, 2H, H-13), 7.29 (d, $J = 8.1$ Hz, 2H, H-14), 7.07 (d, $J = 2.9$ Hz, 1H, H-3), 6.97 (d, $J = 8.8$ Hz, 1H, H-6), 6.80 (dd, $J = 8.8, 2.9$ Hz, 1H, H-5), 2.35 (s, 3H, H-16). ^{13}C NMR (151 MHz, DMSO- d_6) δ 150.55 (C-1), 146.58 (C-4), 142.39 (C-10), 137.75 (C-15), 129.96 (C-12), 128.26 (C-2), 125.72 (C-14), 124.91 (C-13), 122.84 (C-11), 118.32 (C-5), 117.43 (C-3), 111.63 (C-6), 21.35 (C-16); HRMS (APCI) m/z : $[\text{M} + \text{H}]^+$ 268.1096 (Calc. for $\text{C}_{15}\text{H}_{14}\text{N}_3\text{O}_2$: 268.1041); purity (HPLC): 98%.

Methyl 1-(2,5-dihydroxyphenyl)-1H-1,2,3-triazole-4-carboxylate 10

The reaction with methyl propionate produced hybrid **10** as fluffy off white crystals; m.p. 238.0–238.4 °C; IR ν_{max} : 3177, 2953, 1693, 1556, 1475, 1212 cm^{-1} ; ^1H NMR (600 MHz, DMSO- d_6) δ 9.97 (s, 1H, H-4a), 9.36 (s, 1H, H-1a), 9.02 (s, 1H, H-11), 7.07 (d, $J = 2.9$ Hz, 1H, H-3), 6.96 (d, $J = 8.9$ Hz, 1H, H-6), 6.82 (dd, $J = 8.9, 2.8$ Hz, 1H, H-5), 3.88 (s, 3H, H-14). ^{13}C NMR (151 MHz, DMSO- d_6) δ 161.17 (C-12), 150.57 (C-1), 142.40 (C-4), 138.87 (C-10), 130.63 (C-2), 124.09 (C-11), 118.39 (C-5), 118.07 (C-3), 111.48 (C-6), 52.39 (C-14); HRMS (APCI) m/z : $[\text{M} + \text{H}]^+$ 236.0668 (Calc. for $\text{C}_{10}\text{H}_{10}\text{N}_3\text{O}_4$: 236.0627); purity (HPLC): 96%.

2-[4-(Hydroxymethyl)-1H-1,2,3-triazol-1-yl]benzene-1,4-diol 11

The reaction with propargyl alcohol gave hybrid **11** as dark brown crystals; m.p. 228.0–233.6 °C; IR ν_{max} : 3357, 3183, 3085, 1615, 1472 cm^{-1} ; ^1H NMR (600 MHz, DMSO- d_6) δ 9.77 (s, 1H, H-4a), 9.25 (s, 1H, H-1a), 8.33 (s, 1H, H-11), 7.06 (d, $J = 8.7$ Hz, 1H, H-6), 6.93 (d, $J = 2.9$ Hz, 1H, H-3), 6.75 (dd, $J = 8.7, 2.9$ Hz, 1H, H-5), 5.26 (t, $J = 5.3$ Hz, 1H, H-13), 4.60 (d, $J = 4.8$ Hz, 2H, H-12); ^{13}C NMR (151 MHz, DMSO- d_6) δ 150.58 (C-1), 148.16 (C-4), 141.92 (C-10), 124.98 (C-2), 124.49 (C-5), 118.37 (C-11), 117.04 (C-2), 111.17 (C-6), 55.43 (C-12); HRMS (APCI) m/z : $[\text{M} + \text{H}]^+$ 208.0727 (Calc. for $\text{C}_9\text{H}_{10}\text{N}_3\text{O}_3$: 208.0677); purity (HPLC): 98%.

2-[4-(1-Hydroxycyclohexyl)-1H-1,2,3-triazol-1-yl]benzene-1,4-diol 12

The reaction with 1-ethynylcyclohexanol produced hybrid **12** as fluffy off white crystals; m.p. 246.2–247.3 °C; IR ν_{max} : 3263, 3171, 3074, 3025, 2857, 1614, 1494, 1473 cm^{-1} ; ^1H NMR (600 MHz, DMSO- d_6) δ 9.76 (s, 1H, H-4a), 9.25 (s, 1H, H-1a), 8.25 (s, 1H, H-11), 7.09 (d, $J = 2.9$ Hz, 1H, H-3), 6.93 (d, $J = 8.8$ Hz, 1H, H-6), 6.74 (dd, $J = 8.8, 2.9$ Hz, 1H, H-5), 4.98 (s, 1H, H-12a), 1.96–1.83 (m, 4H, H-13 & H-17), 1.82–1.62 (m, 4H, H-14 & H-16), 1.42–1.24 (m, 2H, H-15). ^{13}C NMR (151 MHz, DMSO- d_6) δ 156.15 (C-1), 150.59 (C-4), 141.68 (C-10), 125.03 (C-2), 122.56 (C-11), 118.42 (C-5), 116.86 (C-6), 110.93 (C-3), 68.51 (C-12), 38.26 (C-13, C-17), 25.72 (C-15), 22.10 (C-14, C-16); HRMS (APCI) m/z : $[\text{M} + \text{H}]^+$ 276.1334 (Calc. for $\text{C}_{14}\text{H}_{18}\text{N}_3\text{O}_3$: 276.1303); purity (HPLC): 97%.

2-[4-[[Tetrahydro-2H-pyran-2-yl]oxy]methyl]-1H-1,2,3-triazol-1-yl]benzene-1,4-diol 13

The reaction with tetrahydro-2-(2-propynyloxy)-2H-pyran gave hybrid **13** as brown–red crystals; m.p. 140.1–141.3 °C; IR ν_{max} : 3179, 3084, 2584, 1720, 1614, 1473, 1019 cm^{-1} ; ^1H NMR (600 MHz, DMSO- d_6) δ 9.81 (s, 1H, H-4a), 9.29 (s, 1H, H-1a), 8.45 (s, 1H, H-11), 7.05 (d, $J = 2.9$ Hz, 1H, H-3), 6.93 (d, $J = 8.8$ Hz, 1H, H-6), 6.76 (dd, $J = 8.8, 2.9$ Hz, 1H, H-5), 4.76 (t, $J = 8.5$ Hz, 2H, H-16), 4.59 (t, $J = 9.0$ Hz, 2H, H-12), 3.82 (ddd, $J = 11.6, 8.7, 3.1$ Hz, 1H, H-14), 3.56–3.45 (m, 1H, H-19b), 1.78–1.57 (m, 2H, H-17), 1.57–1.41 (m, 2H, H-18). ^{13}C NMR (151 MHz, DMSO- d_6) δ 150.56 (C-1), 144.07 (C-4), 142.04 (C-10), 125.85 (C-2), 124.84 (C-11), 118.33 (C-5), 117.22 (C-6), 111.32 (C-3), 97.69 (C-14), 61.78 (C-16), 59.89 (C-12), 30.55 (C-19), 25.47 (C-17), 19.47 (C-18); HRMS (APCI) m/z : $[\text{M} + \text{H}]^+$ 292.1314 (Calc. for $\text{C}_{14}\text{H}_{18}\text{N}_3\text{O}_4$: 292.1253); purity (HPLC): 97%.

2-[4-[[Phenylthio]methyl]-1H-1,2,3-triazol-1-yl]benzene-1,4-diol 14

The reaction with phenyl propargyl sulfide afforded hybrid **14** as brown–black crystals; m.p. 151.8–153.0 °C; IR ν_{max} : 3177, 3074, 2595, 1719, 1614 cm^{-1} ; ^1H NMR (600 MHz, DMSO- d_6) δ 9.79 (s, 1H, H-4a), 9.26 (s, 1H, H-1a), 8.33 (s, 1H, H-11), 7.42 (d, $J = 7.7$ Hz, 2H, H-14), 7.33 (t, $J = 7.7$ Hz, 2H, H-15), 7.20 (t, $J = 7.4$ Hz, 1H, H-16), 7.05 (d, $J = 2.9$ Hz, 1H, H-3), 6.93 (t, $J = 8.8$ Hz, 1H, H-6), 6.75 (dd, $J = 8.8, 2.9$ Hz, 1H, H-5), 4.37 (s, 2H, H-12); ^{13}C NMR (151 MHz, DMSO- d_6) δ 150.59 (C-1), 143.77 (C-4), 141.78 (C-10), 136.30 (C-13), 129.49 (C-14, C-18), 128.75 (C-15, C-17), 126.42 (C-2), 124.94 (C-16), 124.74 (C-11), 118.40 (C-5), 117.17 (C-6), 110.95 (C-3), 27.58 (C-12);

HRMS (APCI) m/z : $[\text{M} + \text{H}]^+$ 300.0808 (Calc. for $\text{C}_{15}\text{H}_{14}\text{N}_3\text{O}_2\text{S}$: 300.0807); purity (HPLC): 92%.

Biological evaluation**In vitro antimycobacterial assay**

The minimum inhibitory concentration (MIC) of synthesized compounds was determined using the standard broth micro-dilution method, where a 10 mL culture of *Mycobacterium tuberculosis* (*Mtb*) H37Rv (27294) obtained from American Type Culture Collection (ATCC) (Stringer et al. 2017), was grown to an optical density (OD600) of 0.6–0.7. The growth medium comprised Middlebrook 7H9 base (Difco™) supplemented with 0.03% (v/v) casitone, 0.4% (v/v) glucose, and 0.05% (v/v) tyloxapol (Sigma-Aldrich) as surfactant (Stringer et al. 2017). Cultures grown in the medium were diluted 1:500, prior to inoculation in the MIC assay. The compounds to be tested were reconstituted to a concentration of 10 mM in DMSO. Twofold serial dilutions of the test compounds were prepared across a 96-well microtiter plate, after which, 50 μL of the diluted *Mtb* cultures were added to each well in the serial dilution. Assay controls used were a minimum growth control (Rifampicin (RIF) at $2 \times \text{MIC}$), and a maximum growth control (5% v/v DMSO). The microtiter plates were sealed in a secondary container and incubated at 37 °C with 5% CO_2 and humidification. Relative fluorescence (excitation 485 nM; emission 520 nM) was measured using a plate reader (FLUOstar OPTIMA, BMG LABTECH), at day 7 and day 14. The raw fluorescence data were archived and analysed using the CDD Vault from Collaborative Drug Discovery, in which data were normalized to the minimum and maximum inhibition controls to generate a dose response curve (% inhibition), using the Levenberg–Marquardt damped least squares method, from which the MIC_{90} was calculated (Burlingame, CA www.collaborativedrug.com). The lowest concentration of drug that inhibited growth of more than 90% of the bacterial population was considered the MIC_{90} .

In vitro cytotoxicity assay

The colorimetric MTT [3-(4,5-dimethylthiazol-2-yl)-2,5-diphenyl tetrazolium bromide] assay was developed by Mossman (1983) to measure cytotoxicity and cell proliferation was adopted. Human embryonal kidney, HEK-293 (ATCC CRL-1573). cells were cultured in Dulbecco's modified Eagle's medium with high glucose (Hyclone; Separations) supplemented with 10% fetal bovine serum (Thermofisher Scientific) and 1% L-glutamine (Lonza), 1% penicillin–streptomycin (Lonza), amphotericin B (Lonza), and nonessential amino acids (Lonza). The cells are maintained in a humidified atmosphere at 37 °C and 5% CO_2 . For the MTT assay, 96-well plates (Nunc, Thermofisher Scientific) were

prepared with 200 μL of cell suspension (25,000 cells/mL) and incubated for 24 h. The growth medium was then removed and the cells treated with: (1) 100 μL of emetine dihydrochloride (Sigma-Aldrich) solution diluted with growth medium to the necessary concentrations (positive control); (2) 80 μL of growth medium and 20 μL of solvent (negative control to compensate for possible solvent effects); (3) 80 μL of growth medium and 20 μL of experimental compound solutions. Blanks contained growth medium without cells. The treated plates were incubated for 48 h.

Due to light sensitivity of MTT reagent, the assay was performed in the dark. Sterile-filtered MTT solution (20 μL of 1 mg/mL solution in phosphate-buffered saline (PBS, Sigma-Aldrich)) was added to initiate the MTT assay, the plates covered with aluminum foil and incubated for 4 h. The growth medium-MTT mixture was then aspirated and 100 μL of 2-propanol (Sigma-Aldrich) added to dissolve purple formazan crystals. The contents were gently mixed for 5 min at room temperature. Absorbance was measured at 560 and 650 nm using the Thermofisher Scientific GO Multiscan plate reader. Data analysis was performed for each biological replicate using SkanIt 4.0 Research Edition software. Background absorbance (650 nm) was subtracted from absorbance values (560 nm), the mean absorbance calculated and the percentage cell viability was determined by the following equation:

$$\text{Cell viability \%} = (\Delta \text{ Abs sample} - \Delta \text{ Abs blank}) / (\Delta \text{ Abs neg. control} - \Delta \text{ Abs blank}) \times 100$$

For the final IC_{50} of each compound, the mean IC_{50} of three biological replicates were calculated in GraphPad Prism 5.

In vitro antileishmanial assay

Resazurin assay was adopted to assess the antileishmanial potential of the compounds (Kulshrestha et al. 2013). A brief description is as follows: *Leishmania major* (strain IR-173 (MHOM/IR/-173) obtained through BEI Resources, NIAID, NIH, NR-48816) promastigotes were cultured in M199 with Hank's salts and 0.68 mM L-glutamine (Sigma-Aldrich) supplemented with 4.2 mM NaHCO_3 , 25 mM Hepes (Sigma-Aldrich), 10% fetal bovine serum (Thermofisher Scientific), and 50 U/mL Penicillin/Streptomycin solution (Lonza) and the pH adjusted to 7.3–7.4. The promastigotes were maintained at 26 °C. For the resazurin assay, logarithmic phase promastigotes (1.25×10^5 cells/mL, final volume 100 μL /well) were seeded in 96-well plates (Nunc, Thermofisher Scientific) in the presence of (1) 10 μM of compound for activity screening or (2) 12 twofold dilution concentrations of compounds for IC_{50} determination. Amphotericin B (AMB), 10 μM (Sigma-Aldrich) served as the standard drug and growth medium without parasites served as the blank. The plates were incubated for

72 h at 26 °C in humidified atmosphere. After incubation, 50 μL of resazurin (Sigma-Aldrich) solution (0.01% in PBS) was added to each well and the plates were further incubated at 26 °C in the dark for 4 h. Absorbance was measured at 570 and 600 nm using the Thermofisher Scientific GO Multiscan plate reader. Data analysis was performed for each biological replicate using SkanIt 4.0 Research Edition software. Background absorbance of resazurin (600 nm) was subtracted from the absorbance values of resazurin (570 nm). The mean absorbance calculated and the percentage growth inhibition and cell viability were determined by the following equations:

$$\text{Growth inhibition \%} = \frac{[(\Delta \text{ Abs neg. control} - \Delta \text{ Abs blank}) - (\Delta \text{ Abs sample} - \Delta \text{ Abs blank})]}{(\Delta \text{ Abs neg. control} - \Delta \text{ Abs blank})} \times 100$$

$$\text{Cell viability \%} = (\Delta \text{ Abs sample} - \Delta \text{ Abs blank}) / (\Delta \text{ Abs neg. control} - \Delta \text{ Abs blank}) \times 100$$

The IC_{50} and Z-score were determined for each compound's three biological replicates using GraphPad Prism 5 and the mean IC_{50} of the biological replicates served as the final IC_{50} of each compound.

Statistical analysis

For antimycobacterial activity expressed as MIC_{90} values, statistical analysis was by ANOVA (95% confidence interval) for three biological replicates.

The in vitro cytotoxicity and antileishmanial activity, indicated as IC_{50} values, were derived from nonlinear regression analysis. The results were represented as mean \pm standard error of the mean from three biological replicate experiments. Statistical analysis was performed using SkanIt 4.0 Research Edition software (Thermofisher Scientific) and Prism V5 software (GraphPad). All reported data were significant at $p < 0.05$.

Results and discussion

Chemistry

Considering the interconversion in an aqueous medium between BQ and HQ (Netherlands HCot 2012), the synthetic route adopted occurred in two steps and is depicted in Scheme 2, was described as follows: in the first step (i), 2-azidoquinone, also referred to as azidoquinol, **3** had previously been synthesized (88%) from the reduction of BQ in aqueous acidic medium via Michael addition (Couladourous et al. 1997). The reaction was performed in methanolic acid medium (pH 4), which favored the

reduction of the BQ moiety (Netherlands HCot 2012). In our study, pure instead of aqueous MeOH was used which resulted a marginal increase in yield (89%), and the structure characterization data corroborate this fact.

The viability of this conversion has been tested in biological media with the glutathione (GSH) catalyzed Michael addition of hydroxyquinone to generate S-glutathionyl-HQ reductases (Lam et al. 2012).

In the second step (ii), **3** was reacted with various individual alkynes through copper-catalyzed alkyne-azide cycloaddition (CuCAAC) reaction, or otherwise referred to as click chemistry, to produce different HQ-1,2,3-triazole hybrids. The CuCAAC reaction employed was adapted from a procedure previously reported (Dixit et al. 2012). All synthesized hybrids were produced in poor to moderate yields (23–70%) after purification by recrystallization with hexane. These poor to moderate yields could possibly be explained by the oxidation of HQ to BQ taking place under atmospheric oxygen during the workup but only the corresponding HQ crystallized out (Couladouros et al. 1997).

Structurally, all hybrids differed by the substituent on C-10 of the triazole ring.

The formation of the target compounds was confirmed by routine chemical structure elucidation techniques, NMR (1D), HRMS, and FTIR.

The ^1H NMR spectra of all title compounds were thoroughly examined for characteristic signals, evidence of the HQ and triazole scaffolds. The HQ moiety was clearly identified in ^1H spectra by the presence of two singlets at 9.7 and 9.2 ppm, attributed to quinolic protons H-4a and H-1a, respectively. In addition, two doublets at 6.9 and 7.0 ppm attributed to the resonance of H-3 and H-6, respectively confirm the presence of the quinolic ring. Further, a doublet of doublet in the 6.9–6.7 ppm region, attributed to the resonance of H-5 proton caused by its coupling with H-6 (*ortho*-) and H-3 (*meta*-coupling), was also present in the spectra of all hybrids. The triazole scaffold was clearly identified by the singlet *ca.* 8.2 ppm, which was assigned to the resonance of the triazolyl proton H-11.

^{13}C NMR spectra further confirmed the quinol moiety in the structure of the hybrids as evidenced by the presence of six pronounced peaks in the 150–110 ppm range attributed to the resonance of aryl ring of HQ. Further evidence of the total conversion of BQ to HQ is the absence of carbonyl carbons peaks in the spectra of the hybrids. The ^{13}C spectra, provided further support of the presence of the triazole with two singlet peaks *ca.* 140 and 120 ppm pertaining to the resonance of triazolyl carbons C-10 and C-11, respectively.

The FTIR spectra of all compounds were also inspected for the presence of characteristic absorptions, allowing for the identification of functional groups. The azido (N_3) group of intermediate **3** appeared as small and narrow stretch of relatively low intensity to be peaked up in the

2200–2100 cm^{-1} region (Supplementary information). However, the spectra clearly illustrate the vibration of the OH functional groups of quinol, indicated as variable broad or sharp peaks in 3200–3000 cm^{-1} , and a strong stretch, corresponding with the C = C bond of the triazole moiety in the 1650–1550 cm^{-1} range.

Furthermore, HRMS using APCI ion source show the presence of $[\text{M} + \text{H}]^+$ fragments in the spectra that confirmed the presence of M^+ molecular ion of each hybrid.

Estimated hydrophilicity/lipophilicity balance (CLogP)

In order for the cellular uptake of a drug to occur efficiently through a biological membrane that drug must be neither to lipophilic nor to hydrophilic. Indeed, lipophilic drugs show poor aqueous solubility and tend to be taken up in fatty globules in the intestine. If they reach the blood stream, they may be adsorbed into tissue. Their slow release may exacerbate toxicity such as neurotoxicity. Hydrophilic drugs, on the other hand, may be excreted directly by the kidneys, or should they be able to penetrate a cell membrane, become entrapped in intracellular lipophilic media. Thus, an ideal drug must possess balanced lipophilic/hydrophilic properties to both permeate biological membranes and be taken up for systemic circulation. The *n*-octanol/water partition coefficient (LogP) provides a good measure of this balance with values between 1 and 5 being targeted, and \sim 1–3 being ideal (Lipinski et al. 1997). LogP values were estimated using MarvinSketch 19.4 Software and are gathered in Table 1.

All the hybrids possessed favorable drug-like characteristics with LogP values within the targeted range hence may be biologically active. However, the opposite may also occur on account that biological activity is modulated by many parameters (Pop et al. 2004) aside from physical properties such hydrophilicity, lipophilicity, and their balance thereof.

Biological activities

Before a novel drug can advance to the use in humans, a series of preclinical studies (*viz.* a sequence of *in vitro* assays followed by a series of *in vivo* assays) must be completed (Franzblau et al. 2012). *Mycobacterium* growth inhibitory potential of the hybrids was assessed using a Green Fluorescent Protein-expression assay in a glucose-based Middlebrook 7H9-CAS broth base as protein free growth medium for tubercle *bacilli*.

The MIC of each hybrid that causes 90% inhibition of H37Rv mycobacteria, expressed as MIC_{90} , is shown in Table 1, alongside RIF as antitubercular standard. In addition, HEK-293 cells were used to determine the cytotoxicity of the compounds, alongside cytotoxic drug emetine as reference (Table 1).

Table 1 In vitro biological activities of synthesized hybrids and reference drugs

Compd.	cLogP ^a	Antimycobacterial activity, MIC ₉₀ (μM) ^b	SI ₁	Antileishmanial Activity IC ₅₀ ± SD (μM) ^c	SI ₂	Cytotoxicity IC ₅₀ ± SD (μM) ^d HEK-293
1	0.20	>125		>100		>100
2	0.80	>125		>100		>100
4	2.76	>125		>100		>100
5	3.29	>125		18.28 ± 0.33	6	>100
6	3.82	>125		9.21 ± 0.44	2	17.5 ± 2.1
7	4.88	>125		>100		71.0 ± 7.7
8	3.00	>125		30.26 ± 0.43	3	77.6 ± 7.2
9	3.50	33.84	1	36.49 ± 1.23	1	41.9 ± 7.9
10	1.21	>125		>100		>100
11	-0.12	>125		>100		>100
12	1.89	>125		71.29 ± 0.65	1	>100
13	1.20	>125		>100		>100
14	3.03	16.38	6	22.68 ± 0.74	4	>100
RIF	3.71	0.075				
AMB				0.03 ± 0.006		
EM						0.01 ± 0.001

EM emetine, AMB amphotericin B

Experiments were run in triplicate and all reported data were significant at $p < 0.05$

^acLogP values calculated using MarvinSketch Version 19.4

^bCompounds screened in protein free medium 7H9 GLU CAS against H37Rv strain

^cCompounds screened against *L. major* IR-175 strain

^dHEK-293: human embryonic kidney cell line

^eSelectivity index (SI), $SI_1 = IC_{50} \text{ HEK-293}/MIC_{90} \text{ H37Rv}$, $SI_2 = IC_{50} \text{ HEK-293}/MIC_{50} \text{ L. major}$

The antileishmanial activity of synthesized compounds was evaluated mainly against *L. major* strain IR-175, which communicates CL. The susceptibility of the compounds to the promastigotes (infective stage) was assessed through determination of the IC₅₀ values. The half maximal inhibitory concentration (IC₅₀) is a measure of the potency of a substance in inhibiting a specific biological or biochemical function. IC₅₀ is a quantitative measure that indicates how much of a particular inhibitory substance (e.g., drug) is needed to inhibit, in vitro, a given biological process or biological component by 50%. In this study, antileishmanial IC₅₀ values determination was achieved using the resazurin assay, also known as the AlamarBlue® assay, which involves the irreversible enzymatic reduction of oxidized blue resazurin dye to pink, highly fluorescent resorufin by viable cells (Kulshrestha et al. 2013). The IC₅₀ data of synthesized hybrids are shown in Table 1, alongside that of AMB as antileishmanial standard.

The hybrids were screened as solutions.

Antimycobacterial activity

None of the hybrids in the series possessed notable antimycobacterial activity. All *n*-alkyl chain hybrids were inactive and so were the precursor scaffolds, *p*-BQ and HQ

with MIC₉₀ values greater than 125 μM. Only compounds **9** and **14** had MIC₉₀ values below 125 μM, and thus were considered active. Antimycobacterial active hybrid **9** had a methyl group in *para* position of the aryl ring. Removal of that group resulted in the completely loss of activity (**8** IC₅₀ > 125 μM). Hybrid **14**, on the other hand, had phenylthio-methyl moiety.

Furthermore, hybrids **10** and **13** had electron withdrawing and donating group, respectively, and yet were inactive.

The unique lipid rich (Glickman and Jacobs 2001; Knechel 2009) cell wall structure of *Mycobacterium* is crucial for survival of the pathogen (Knechel 2009). Thus, lipophilicity is an imperative consideration in the design and activity of novel antimycobacterial drugs (Suresh et al. 2014). The antimycobacterial activity can therefore be enhanced by improving the lipophilic property of a compound hence the selection of lipophilic moieties in this study in order to facilitate diffusion of the compounds through biomembranes.

All synthesized hybrids showed favorable drug-like properties (except **11**) having cLogP values in the targeted range, and thus were expected to be efficiently transported into the *Mycobacterium* through passive diffusion. However, none of them displayed significant activity against

Mtb. This suggests that lipophilicity did not modulate the antimycobacterial activity of the hybrids, which is in accordance with previous findings (Zhang et al. 2017)

BQ 1, HQ 2, and the hybrids (exception of 6–9) in general showed no toxicity to the HEK-293 cells. Hybrids 6–9 displayed moderate to mild toxicity ($10 < IC_{50} < 50 \mu M$) (Liu et al. 2017), which may be attributed to their relatively higher lipophilicity with cLogP values, varying in the 3–5 range. In the *n*-alkyl chain substituted sub-series, the short chain containing hybrids 4 ($n = 4$) and 5 ($n = 5$) were found to be noncytotoxic. However, a further increase in chain length resulted in a cytotoxicity decrease, with 6 (6C; MIC_{50} 17.5 μM) being more cytotoxic than 7 (8C; MIC_{50} 71.0 μM). Hybrids 6 and 7 possessed moderate and mild toxicities, respectively.

The most antimycobacterial active hybrid 14 (MIC_{90} 16.38 μM) showed no toxicity to HEK-293 cells, but had a poor selectivity toward the bacteria ($SI = 6$). All together, these biological features disqualify this hybrid as a potential antimycobacterial hit (Katsuno et al. 2015).

Antileishmanial activity

Leishmania spp. have two developmental forms, promastigote and amastigote. The former is responsible for the infective stage while the latter accounts for the clinical stage, and is thus liable for the clinical manifestations of the disease. In this study, a systematic approach, which consists of evaluating the compounds in primary promastigote screen then select potential hits for further intracellular anti-amastigote activity (intra-macrophage) screening was adopted. The former screen targeting the free living and easily cultured promastigote while the latter targets the clinically relevant but more difficult to culture intra-macrophage amastigote. Furthermore, promastigote screen, although more suitable for automation, fails to identify all active compounds and leads to numerous false positive hits (De Muylder et al. 2011). Indeed, only 4% anti-promastigote hits are confirmed in anti-amastigote (Siqueira-Neto et al. 2012) screening, which infers that an anti-amastigote hit is a potential anti-promastigote hit while the opposite may not be certain (De Muylder et al. 2011).

Half of the hybrids showed activity against the promastigotes. Thus, the parasites were more susceptible to the hybrids than were the bacteria. However, the observed antiparasitic activity may not be fully intrinsic but possibly also stemming from systemic toxicity for some of the compounds. Indeed, those that were moderately to weakly toxic ($20 < IC_{50} < 80 \mu M$) on the mammalian cell line (Liu et al. 2017), had poor selectivity indexes ranging from 1 to 6. The best performer was hybrid 6, 2-(4-Hexyl-1*H*-1,2,3-triazol-1-yl)benzene-1,4-diol, with IC_{50} 9.21 μM , featured 6C side chain on the triazole ring, and displayed poorly

selective antiparasitic action ($SI = 2$). The 5C side chain hybrid 5, on the other hand, had twice lower activity (IC_{50} 18.28 μM) and was noncytotoxic to HEK-293 cells ($IC_{50} > 100 \mu M$) but was found to be comparatively selective ($SI = 6$) toward the parasites. Neither of them stood as hit antileishmanial, not only on account of cellular potency ($IC_{50} < 10 \mu M$) and selectivity index ($SI < 10$) but also on pathogenesis consideration as *L. major* promastigote is herein investigated instead of *L. donovani* amastigote as recommended by Katsuno et al. (2015).

Conclusions

A small library of HQ-1,2,3-triazole hybrids was synthesized in poor to moderate yield following a two-step process that involves acid-catalyzed Michael and copper-catalyzed azide-alkyne [3 + 2] cycloaddition. The anti-infective properties namely antimycobacterial and antileishmanial activities of the hybrids were evaluated in vitro against human virulent *Mtb* H37Rv and *L. major* promastigotes, respectively. The cytotoxicity of the compounds was also assessed using HEK-293 cells. Though all hybrids showed good drug-like properties, they were found to be mostly inactive. The most active hybrid, 14 featuring phenylthio-methyl moiety, although nontoxic to mammalian cells, possessed moderate activities against bacteria (MIC_{90} 16.38 μM) and parasite (IC_{50} 22.68 μM) and poor pathogenic selective action ($SI = 4–6$). Thus, neither antitubercular nor antileishmanial hit was discovered during this study.

A common structural characteristic of the hybrids of this library is rigidity. Thus, more compounds will be needed to determine if rigidity indeed governs the biological performance of these hybrids. Future work will also focus on the investigation of flexible hybrids containing the two pharmacophores in comparison with rigid ones.

Acknowledgements The authors thank Dr D. Otto for NMR and Dr JHL Jordaan for MS analyses. The following reagent was obtained through BEI Resources, NIAID, NIH: *Leishmania major*, Strain IR-173 (MHOM/IR/173), NR-48816.

Funding This work was funded by South African National Research Foundation Grant to DDN (UID 98937 and 115349) and the North-West University. All TB screening work in the MMRU (UCT) is supported by the South African Medical Research Council (SAMRC) with funds from the South African National Treasury under its Economic Competitiveness and Support Package through the Strategic Health Innovation Partnerships (SHIP) initiative (to DFW).

Author contributions Conceptualization: DDN; methodology: [C-MH, JA, FJS, RS, AJ, and DFW]; formal analysis and investigation: DDN, JA, and DFW; writing original draft preparation: C-MH; writing, reviewing and editing: DDN; funding acquisition: DDN and DFW; resources: DDN and DFW; supervision: DDN.

Compliance with ethical standards

Conflict of interest The authors declare that they have no conflict of interest.

Ethical approval This research project was conducted under the institutional ethical approval NWU-00141-14-A5.

Publisher's note Springer Nature remains neutral with regard to jurisdictional claims in published maps and institutional affiliations.

References

- Ali AA et al. (2017) Synthesis and biological evaluation of novel 1,2,3-triazole derivatives as anti-tubercular agents. *Bioorg Med Chem Lett* 27:3698–3703
- Amir A, Rana K, Arya A, Kapoor N, Kumar H, Siddiqui MA (2014) *Mycobacterium tuberculosis* H37Rv: in silico drug targets identification by metabolic pathways analysis. *J Evol Biol* 2014:8
- Ansari MY, Dikhit MR, Sahoo GC, Ali V, Das P (2017) Recent advancement and treatment of leishmaniasis based on pharmacoinformatics approach: current and future outlook. *Gene Rep* 9:86–97
- Aronson N et al. (2017) Diagnosis and treatment of leishmaniasis: clinical practice guidelines by the Infectious Diseases Society of America (IDSA) and the American Society of Tropical Medicine and Hygiene (ASTMH). *Am J Trop Med Hyg* 96:24–45
- Boechat N et al. (2011) Novel 1,2,3-triazole derivatives for use against *Mycobacterium tuberculosis* H37Rv (ATCC 27294) strain. *J Med Chem* 54:5988–5999
- Brotherton M-C, Bourassa S, Légaré D, Poirier GG, Droit A, Ouellette M (2014) Quantitative proteomic analysis of amphotericin B resistance in *Leishmania infantum*. *Int J Parasitol Drugs Drug Resist* 4:126–132
- CDC (2018a) CDC | TB | Data and statistics. <https://www.cdc.gov/tb/statistics/default.htm>. Accessed 25 July 2018
- CDC (2019) Resources for health professionals. https://www.cdc.gov/parasites/leishmaniasis/health_professionals/index.html#tx. Accessed 9 Feb 2020
- Couladouros EA, Plyta ZF, Haroutounian SA, Papageorgiou VP (1997) Efficient synthesis of aminonaphthoquinones and azido-benzohydroquinones: mechanistic considerations of the reaction of hydrazoic acid with quinones. An overview. *J Org Chem* 62:6–10
- De Muylder G, Ang KKH, Chen S, Arkin MR, Engel JC, McKerrow JH (2011) A screen against *Leishmania* intracellular amastigotes: comparison to a promastigote screen and Identification of a host cell-specific hit. *PLOS Negl Trop Dis* 5:e1253
- Deep DK et al. (2017) Increased miltefosine tolerance in clinical isolates of *Leishmania donovani* is associated with reduced drug accumulation, increased infectivity and resistance to oxidative stress. *PLoS Negl Trop Dis* 11:e0005641
- Dixit SK, Mishra N, Sharma M, Singh S, Agarwal A, Awasthi SK, Bhasin VK (2012) Synthesis and in vitro antiparasitoid activities of fluoroquinolone analogs. *Eur J Med Chem* 51:52–59
- du Toit LC, Pillay V, Danckwerts MP (2006) Tuberculosis chemotherapy: current drug delivery approaches. *Respir Res* 7:118
- Franzblau SG et al. (2012) Comprehensive analysis of methods used for the evaluation of compounds against *Mycobacterium tuberculosis*. *Tuberculosis* 92:453–488
- Glickman MS, Jacobs WR (2001) Microbial pathogenesis of *Mycobacterium tuberculosis*: dawn of a discipline. *Cell* 104:477–485
- Hadighi R, Mohebbi M, Boucher P, Hajjarian H, Khamesipour A, Ouellette M (2006) Unresponsiveness to glucantime treatment in Iranian cutaneous leishmaniasis due to drug-resistant *Leishmania tropica* parasites. *PLoS Med* 3:e162
- Jyoti MA, Nam K-W, Jang WS, Kim Y-H, Kim S-K, Lee B-E, Song H-Y (2016) Antimycobacterial activity of methanolic plant extract of *Artemisia capillaris* containing ursolic acid and hydroquinone against *Mycobacterium tuberculosis*. *J Infect Chemother* 22:200–208
- Katsuno K et al. (2015) Hit and lead criteria in drug discovery for infectious diseases of the developing world. *Nat Rev Drug Discov* 14:751–758
- Knechel NA (2009) Tuberculosis: pathophysiology, clinical features, and diagnosis. *Crit Care Nurse* 29:34–43
- Kulshrestha A et al. (2013) Validation of a simple resazurin-based promastigote assay for the routine monitoring of miltefosine susceptibility in clinical isolates of *Leishmania donovani*. *Parasitol Res* 112:825–828
- Kumar D, Beena, Khare G, Kidwai S, Tyagi AK, Singh R, Rawat DS (2014a) Synthesis of novel 1,2,3-triazole derivatives of isoniazid and their in vitro and in vivo antimycobacterial activity evaluation. *Eur J Med Chem* 81:301–313
- Lam LKM, Zhang Z, Board PG, Xun L (2012) Reduction of benzoquinones to hydroquinones via spontaneous reaction with glutathione and enzymatic reaction by S-glutathionyl-hydroquinone reductases. *Biochemistry* 51:5014–5021
- Lindsey RH, Bromberg KD, Felix CA, Osheroff N (2004) 1,4-Benzoquinone is a topoisomerase II poison. *Biochemistry* 43:7563–7574
- Lipinski CA, Lombardo F, Dominy BW, Feeney PJ (1997) Experimental and computational approaches to estimate solubility and permeability in drug discovery and development settings. *Adv Drug Deliv Rev* 23:3–25
- Liu S, Su M, Song S-J, Jung HJ (2017) Marine-derived *Penicillium* species as producers of cytotoxic metabolites. *Mar Drugs* 15:329
- Mairet-Khedim M et al. (2019) In vitro activity of ferroquine against artemisinin-based combination therapy (ACT)-resistant *Plasmodium falciparum* isolates from Cambodia. *J Antimicrob Chemother* 74:3240–3244
- McGregor D (2007) Hydroquinone: an evaluation of the human risks from its carcinogenic and mutagenic properties. *Crit Rev Toxicol* 37:887–914
- Mosmann T (1983) Rapid colorimetric assay for cellular growth and survival: application to proliferation and cytotoxicity assays. *J Immun Methods* 65:55–63
- Netherlands HCot (2012) Benzoquinone and hydroquinone: health-based recommended occupational exposure limit. <https://slidertips/download/health-council-of-the-netherlands-hydroquinone-and-benzoquinone>. Accessed 10 Oct 2018
- Ponte-Sucre A et al. (2017) Drug resistance and treatment failure in leishmaniasis: a 21st century challenge. *PLoS Negl Trop Dis* 11:e0006052
- Pop E, Oniciu DC, Pape ME, Cramer CT, Dasseux J-LH (2004) Lipophilicity parameters and biological activity in a series of compounds with potential cardiovascular applications. *Croat Chem Acta* 77:301–306
- Sagnou M, Strongilos A, Hadjipavlou-Litina D, Couladouros EA (2009) Synthesis of novel benzoquinones with anti-inflammatory activity. *Lett Drug Des Discov* 6:172–177
- Siqueira-Neto JL et al. (2012) An image-based high-content screening assay for compounds targeting intracellular *Leishmania donovani* amastigotes in human macrophages. *PLoS Negl Trop Dis* 6:e1671
- Smit FJ, N'Da DD (2014) Synthesis, in vitro antimalarial activity and cytotoxicity of novel 4-aminoquinolinyl-chalcone amides. *Bioorg Med Chem* 22:1128–1138
- Smit FJ, Seldon R, Aucamp J, Jordaan A, Warner DF, N'Da DD (2019) Synthesis and antimycobacterial activity of disubstituted benzyltriazoles. *Med Chem Res* 28:2279–2293

- Smit FJ, van Biljon RA, Birkholtz L-M, N'Da DD (2015) Synthesis and in vitro biological evaluation of dihydroartemisinin-chalcone esters. *Eur J Med Chem* 90:33–44
- Souček P, Ivan G, Pavel S (2000) Effect of the microsomal system on interconversions between hydroquinone, benzoquinone, oxygen activation, and lipid peroxidation. *Chem-Biol Interact* 126:45–61
- Stringer T et al. (2017) Antimicrobial activity of organometallic isonicotinyl and pyrazinyl ferrocenyl-derived complexes. *Dalton Trans* 46:9875–9885
- Suresh N, Nagesh HN, Renuka J, Rajput V, Sharma R, Khan IA, Kondapalli Venkata Gowri CS (2014) Synthesis and evaluation of 1-cyclopropyl-6-fluoro-1,4-dihydro-4-oxo-7-(4-(2-(4-substitutedpiperazin-1-yl)acetyl)piperazin-1-yl)quinoline-3-carboxylic acid derivatives as anti-tubercular and antibacterial agents. *Eur J Med Chem* 71:324–332
- Tasdemir D, Brun R, Yardley V, Franzblau SG, Rüedi P (2006) Antitubercular and antiprotozoal activities of primin, a natural benzoquinone: In vitro and in vivo studies. *Chem Biodivers* 3:1230–1237
- Torres-Guerrero E, Quintanilla-Cedillo MR, Ruiz-Esmenjaud J, Arenas R (2017) Leishmaniasis: a review. *F1000Res* 6:750
- Tran T, Saheba E, Arcerio AV, Chavez V, Li Q-Y, Martinez LE, Primm TP (2004) Quinones as antimycobacterial agents. *Bioorg Med Chem* 12:4809–4813
- Valderrama JA, Zamorano C, Gonzalez MF, Prina E, Fournet A (2005) Studies on quinones. Part 39: synthesis and leishmanicidal activity of acylchloroquinones and hydroquinones. *Bioorg Med Chem* 13:4153–4159
- Viegas-Junior C, Danuello A, da Silva Bolzani V, Barreiro EJ, Fraga CAM (2007) Molecular hybridization: a useful tool in the design of new drug prototypes. *Curr Med Chem* 14:1829–1852
- WHO (2018a) WHO | TB | Key facts. <http://www.who.int/en/news-room/fact-sheets/detail/tuberculosis>. Accessed 25 July 2018
- WHO (2018b) Global health observatory (GHO) data. <http://www.who.int/gho/tb/en/>. Accessed 25 July 2018
- WHO (2018c) Global TB report 2018. https://www.who.int/tb/publications/global_report/en/. Accessed 10 Oct 2018
- WHO (2018d) Leishmaniasis: situation and trends. http://www.who.int/gho/neglected_diseases/leishmaniasis/en/. Accessed 16 July 2018
- WHO (2018e) Leishmaniasis. <http://www.who.int/news-room/fact-sheets/detail/leishmaniasis> Accessed 5 Mar 2018
- WHO (2019f) Leishmaniasis: the disease. <https://www.who.int/leishmaniasis/disease/en/>. Accessed 9 Feb 2020
- WHO (2019g) Leishmaniasis: key facts. <https://www.who.int/news-room/fact-sheets/detail/leishmaniasis>. Accessed 9 Feb 2020
- Zhang S, Xu Z, Gao C, Ren Q-C, Chang L, Lv Z-S, Feng L-S (2017) Triazole derivatives and their anti-tubercular activity. *Eur J Med Chem* 138:501–513